SECTION 4

RESPONSE OF INTERIOR CONNECTIONS

The behavior of interior slab-column connections observed during the tests is presented in this chapter. The discussion is focused on cracking pattern and strain distribution in the slab, failure mode, moment-rotation response, stiffness degradation, and moment-transfer capacity of the interior connections.

4.1 Cracking Pattern

Flexural cracks on the top surface of the slab at interior connections in all specimens initially developed normal to the loading direction and extended over a limited width of the slab. As the drift level increased, these cracks grew both in width and length and became more inclined to the direction of loading. The final configuration of the cracking pattern on the top surface of the slab for all specimens is shown in figure 4-1. Except for the cracks adjacent to the column face, the other flexural cracks tended to radiate away from the column periphery.

The cracks on the bottom surface of the slab showed more dependence on the slab reinforcing detail and the intensity of the gravity load. When gravity load was present, the net positive moment developed a certain distance away from the column face. The termination of the bottom reinforcing bars short of the interior column in bent-up detail, therefore, had less severe consequence under load reversals. The positive moment in the slab in DNY_2, which carried a high gravity load, developed even farther away from the column face. In straight bar detail, as in DNY_3, half of the slab bottom reinforcement was cut short of the column face and the remaining half continued into the column. This detail created a potential for cracking where the reinforcement was terminated. The specimen DNY_3 was subjected to a large initial displacement due to a malfunction in the control circuitry which resulted in a flexural crack on the bottom of the slab at the column face. The second flexural crack developed approximately at the location of the cut-off point of the slab positive reinforcement.

4.2 Strain Distribution

The distribution of strain in the slab top reinforcement at interior connections is shown in figure 4-3. The presence of spandrel beams at exterior connections and configuration of the slab reinforcing detail do not appear to have significant affect on the distribution of strain in the slab top reinforcement at interior connections. The slab reinforcement within the column strip in all specimens was uniformly distributed. The slab top reinforcement therefore yielded over a larger width of C_1+5h centered on the column line. The transfer of unbalanced moment at interior connections was ob-

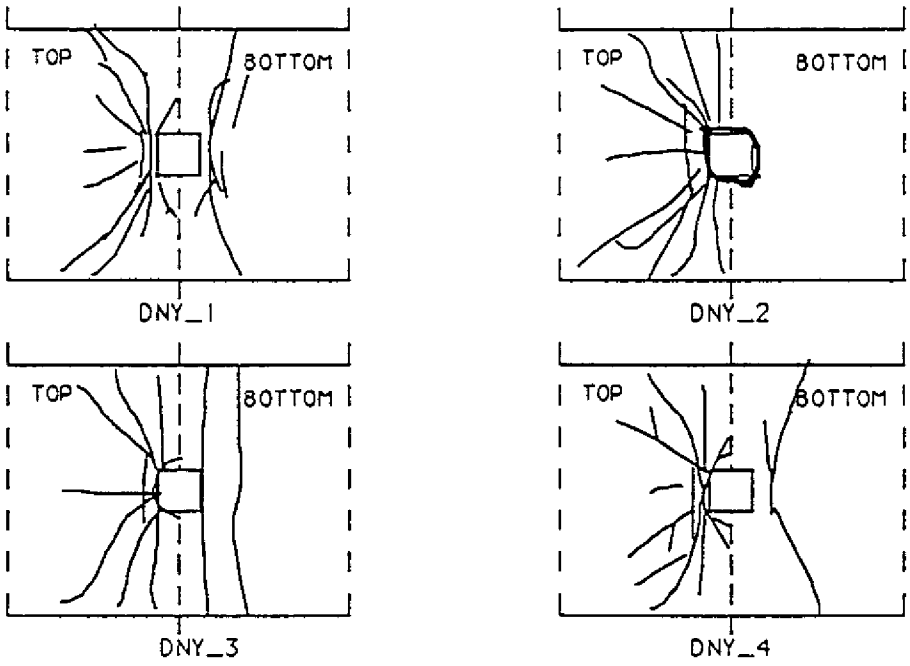

FIGURE 4-1 Cracking Pattern of Interior Connections

FIGURE 4-2 Punching Failure of Interior Connection in DNY_2

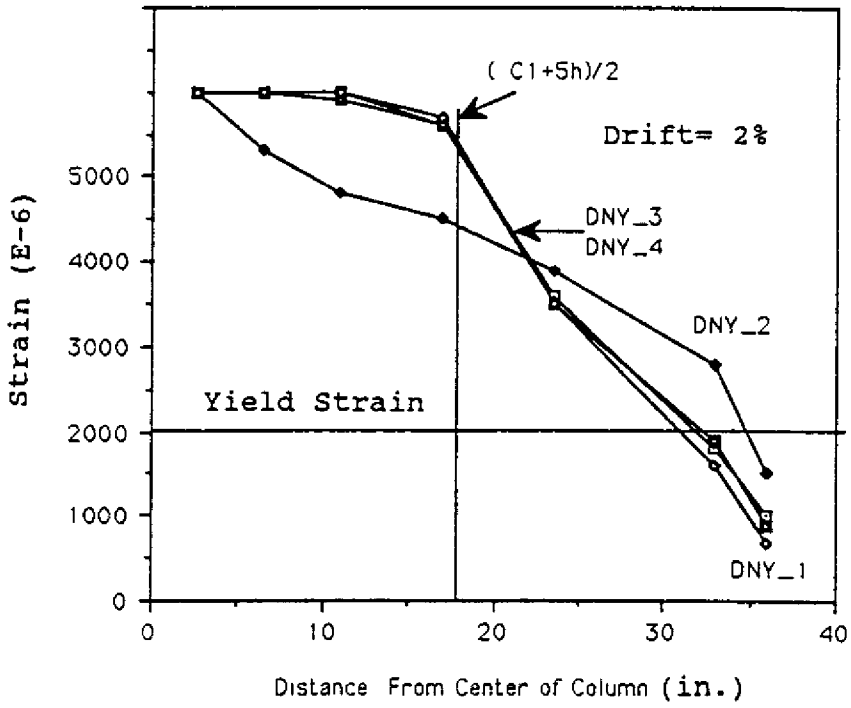

FIGURE 4-3 Strain Distribution at Interior Connection of Specimens

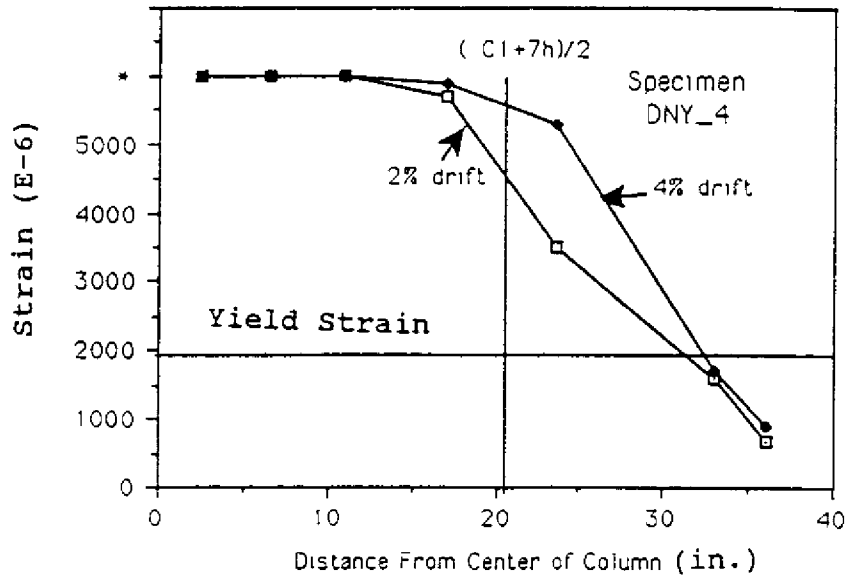

FIGURE 4-4 Strain Distribution at Interior Connection in DNY_4

served to occur mostly over this width, which may be regarded as the effective width of the slab. Once the slab cracked under positive bending, the transfer of unbalanced moment occurred only on the side of the column with slab top reinforcement in tension. This further enlarged the slab effective width to approximately C_1+7h., as shown in figure 4-4.

4.3 Failure Mode

Among all the specimens, only the interior connection of DNY_2 failed in punching due to high gravity shear at a relatively small drift of 2%. The resulting failure surface is shown in figure 4-2. The interior connection of DNY_4 sustained large lateral drift and appeared to fail in punching towards the end of the test at about 5% drift. The interior connections of DNY_1 and DNY_3 experienced flexural yielding mechanism which resulted in a relatively large rotation of the slab.

4.4 Moment-Rotation Response

The moment-rotation response of interior connections was derived from the forces measured at the top and bottom of the interior column and the rotation of the slab over a distance of 6 inches from the column face. Figures 4-5 and 4-6 show the moment-rotation loops for the specimens DNY_1 and DNY_2, respectively. The moment causing tension on the top of the slab is indicated as positive moment in these plots. Because of the small amount of reinforcement or no reinforcement at the bottom of the slab in the connection region, the negative moment capacity was limited to the cracking moment of the slab. The location of the cracking moment under positive bending, however, varied with the level of gravity load. Because of the net negative moment at the interior connection, the positive moment in the slab and hence the cracking moment occurred a certain distance away from the column face. The rotation of the slab measured over a distance of six inches from the column face could vary significantly depending upon the magnitude of the gravity load. The difference in the initial stiffness between the positive and negative loading directions is attributed to initial cracking of the slab in the connection region due to the superimposed gravity load. The bilinear shape of the envelope for the loading direction causing tension in the slab top reinforcement was typical of all specimens. The moment capacity in the opposite direction was mostly limited to cracking strength of the slab. Once the slab reached its cracking capacity, the moment degraded rapidly depending upon the anchorage condition and the location of the flexural cracks relative to column on the bottom face of the slab.

4.5 Stiffness Degradation

The loss of connection stiffness under lateral loading can be critical to the performance of non-ductile flat-plate buildings. Because of the distinctly different reinforcing amount and detail in the top and bottom of the slab, the rate of loss of stiffness in the two directions was also quite different. Figure 4-7 shows the loss of stiffness experienced by the specimens at different drift levels. The

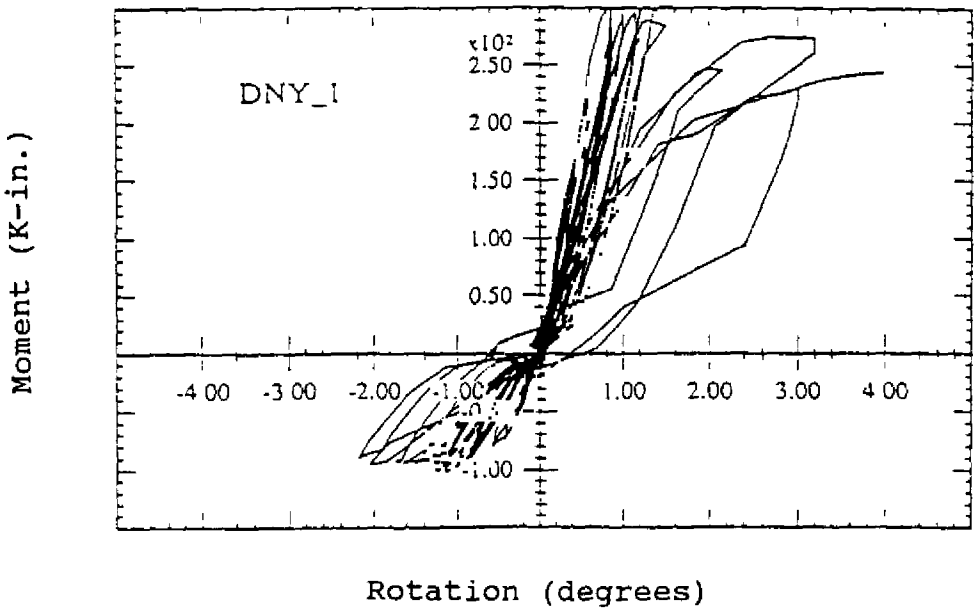

FIGURE 4-5 Moment-Rotation of Interior Connection of DNY_1

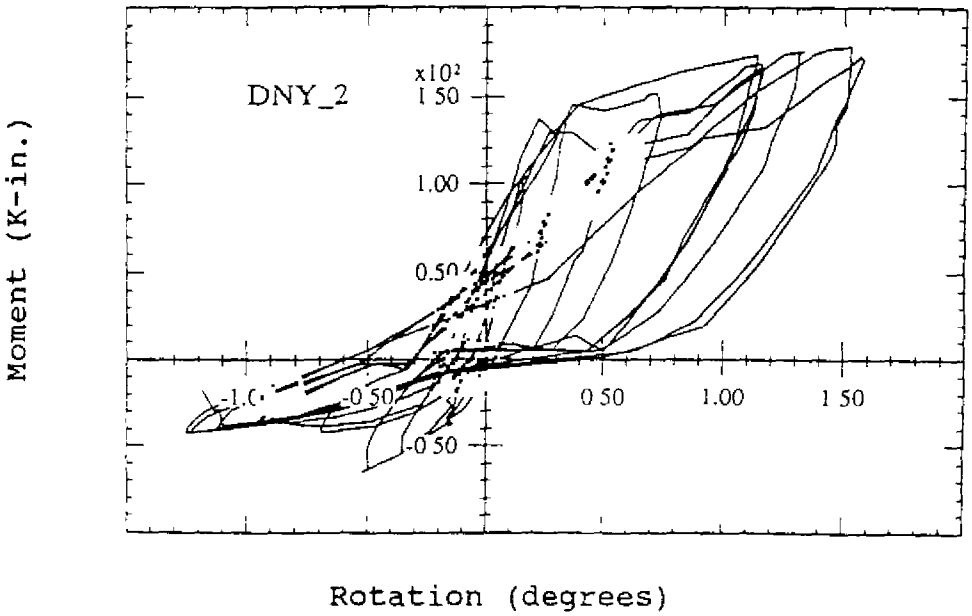

FIGURE 4-6 Moment-Rotation of Interior Connection of DNY_2

stiffness of the connection here is assumed as moment per unit rotation of the slab in the connection region.

The initial stiffness in the loading direction causing tension in the slab top reinforcement was significantly higher than the initial stiffness in the loading direction causing tension in the slab bottom reinforcement. The rate of loss of stiffness for the specimens with the same level of gravity load was roughly the same. Up to 2% drift, the stiffness of the specimens degraded rapidly losing approximately 75 to 85% of the initial stiffness.The loss of stiffness beyond this drift level was more gradual. Due to initial cracking of the slab from higher gravity load, the initial stiffness of specimen DNY_2 was lower. Its stiffness degraded in a manner similar to the other specimens upto 1% drift. Beyond this drift level, the stiffness of DNY_2 dropped rapidly due to the impending punching failure. In the opposite loading direction, the stiffness degraded much more rapidly becoming negligible as soon as the slab reached its cracking capacity and the slab bottom reinforcement lost its anchorage.

4.6 Moment-Transfer Capacity

The moment transfer capacity of the slab in the two loading directions was significantly different due to the different amounts of slab top and bottom reinforcement. As such the two cases are discussed separately.

SLAB TOP IN TENSION

The moment causing tension in the slab top reinforcement was resisted mostly within the slab width equal to the column strip. The strain in reinforcement within this width was much higher compared to the strain in reinforcement in the remaining width of the slab. The design of interior connections required 75% of the total reinforcement to be placed within the column strip. The assumption of column strip as the effective width for calculation of bending moment gives a conservative estimate of the bending capacity. The actual moment transferred by the slab and the theoretical flexural strength of the column strip are given in table 4-I. The observed moments are about 10% higher than the flexural capacity of the column strip. The slab in specimen DNY_2 did not reach its full flexural strength due to early punching failure of the connection. The moment transfer capacity of the slab under negative bending could therefore be conservatively taken as the flexural capacity of the slab column strip.

SLAB BOTTOM IN TENSION

The moment transfer capacity of the interior connection under positive bending depended a great deal on the detail of the slab bottom reinforcement. In the bent-up reinforcing detail, all the slab

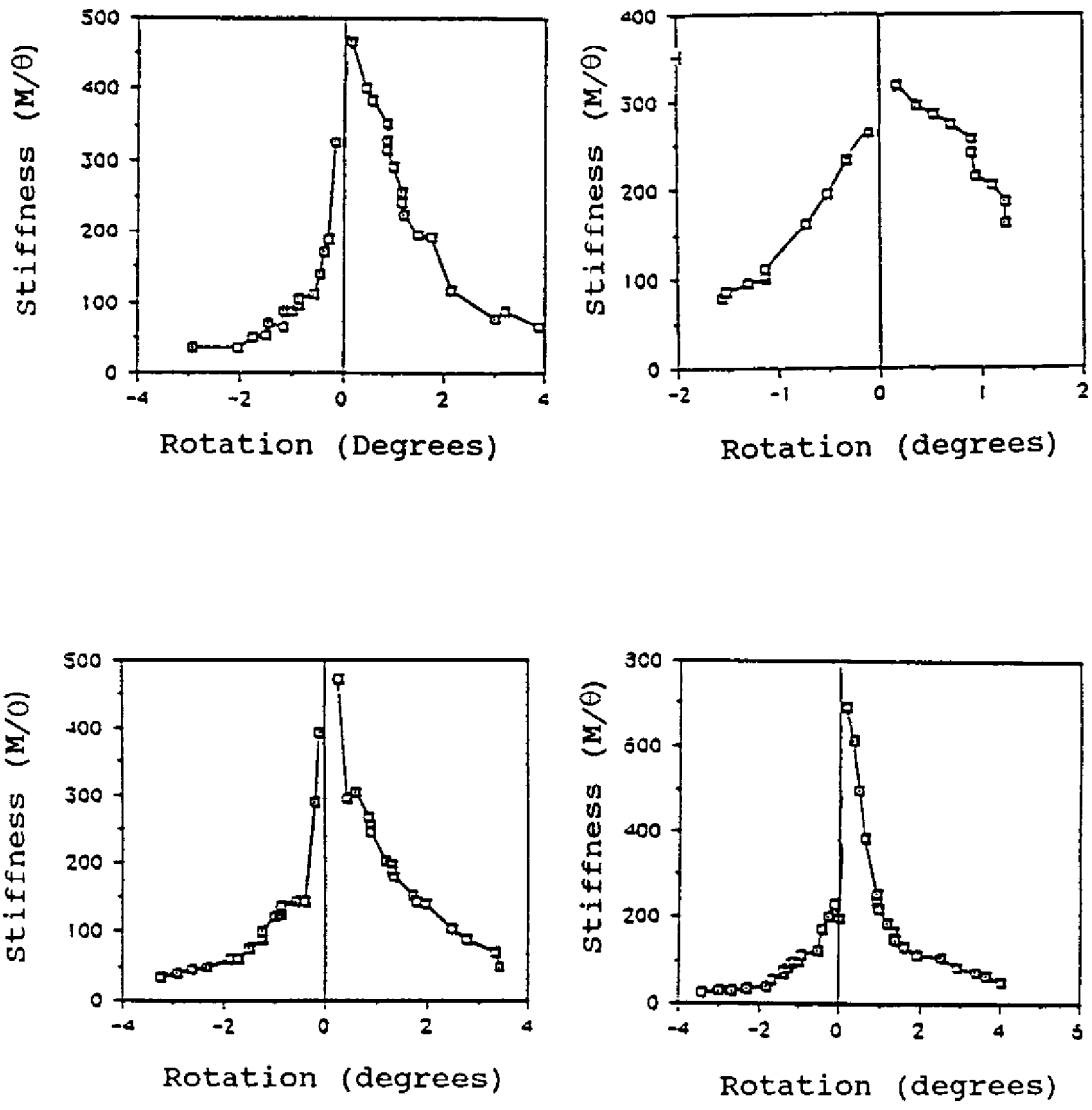

FIGURE 4-7 Stiffness Degradation of Interior Connections

bottom reinforcement was either bent-up or stopped short of the column. The slab, therefore, had no reinforcement at the bottom face adjacent to the column. In the region between the cut-off point and the bent-up point, the amount of reinforcement was less than the minimum reinforcement requirement. Even though the flexural cracking did not occur at the face of the column due to the presence of the gravity load, the maximum moment-transfer was limited to flexural cracking strength of the slab. In straight bar reinforcing detail of the slab, 50% of the slab bottom reinforcement was terminated at six inches from the column face and the remaining reinforcement extended three inches beyond the column center line. The amount of reinforcement continuing into the column is typically less than the minimum reinforcement requirement. The moment-transfer capacity of the slab with straight bar detail was also limited to the slab cracking strength. Once the slab reached its cracking strength under positive bending, the slab reinforcement immediately yielded or lost its anchorage reducing the moment-transfer capacity to almost zero.

TABLE 4-I Moment Transfer Capacity of Interior Connections

Specimens	M_m* (k-in.)	M_{mf}† (k-in.)	M_{un}‡ (k-in.)	M_{mf}/M_n**
DNY_1	320	275	418	1.07
DNY_2	270	233	296	0.85
DNY_3	360	284	428	1.10
DNY_4	332	269	390	0.92

*. measured maximum moment at centroid of connection
†. measured maximum moment at column face
‡. measured maximum unbalanced moment at connection
**. calculated nominal moment capacity of slab

SECTION 5

RESPONSE OF EXTERIOR CONNECTIONS

The behavior of exterior slab-column connections is presented in this section. The discussion is focused on the observed cracking pattern, strain distribution in the slab reinforcement, failure mode, stiffness and moment-rotation relationship. The ability to transfer the unbalanced moment, both in the positive and negative moment directions, and the effective width of the slab are discussed in greater detail.

5.1 Cracking Pattern

Initial cracking of the slab in the connection region depended upon the magnitude of the gravity load applied to the slab before the start of each test. Specimens DNY_1, DNY_3, DNY_4 were subjected to full dead load plus thirty percent of the live load. Only the specimen DNY_2, which carried the full design dead and live load, experienced initial cracking. These cracks first appeared at the face of the exterior column as flexural cracks which were joined by torsional cracks extending from inside corners of the column to the slab edge at about forty five degrees angle. During the initial cycles, the flexural and torsional cracks elongated and increased in width with only a few new cracks. By 1.0% drift, the flexural crack at the bottom of the slab, adjacent to the exterior column, had extended the full slab width in specimens DNY_1 and DNY_4. Because of the straight bar detail in DNY_3, the flexural and torsional cracks both on the top and bottom of the slab were very similar up to 2% drift. These cracks opened wider as the drift increased. The location, length and width of the flexural crack on the bottom of the slab was affected by the magnitude of the gravity load on the slab. In specimen DNY_2, which supported the heaviest gravity load, the major flexural crack on the bottom of the slab occurred 22 inches away from the column face at 2% drift. In other specimens, such crack developed closer to the column. Since only a small amount of the slab bottom reinforcement in bent-up detail extended into the column, these cracks tended to be more severe. The final cracking patterns at exterior connections of the four specimens are shown in figure 5-1 The torsional cracks in the spandrel beam of DNY_4 were very minimal. Unlike in other specimens, a yield line developed across the full width of the slab at the face of the spandrel beam under negative bending as shown in figure 5-2.

5.2 Strain Distribution

The distribution of strain in the slab top reinforcement under negative moment is of interest in determining the slab participation during the transfer of unbalanced moment. The distribution of strain in the slab top reinforcement at first yield and at peak load for each specimen are shown in figures 5-3 and 5-4, respectively. The presence of a spandrel beam in DNY_4 resulted in a more

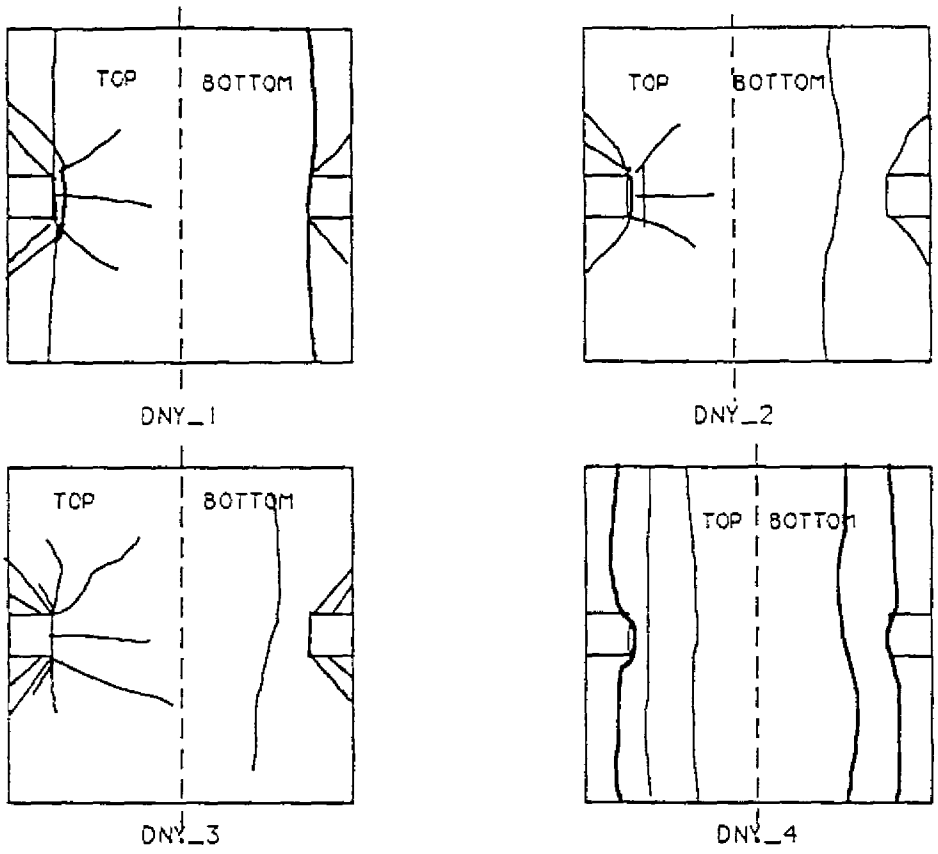

FIGURE 5-1 Cracking Pattern of Exterior Connections

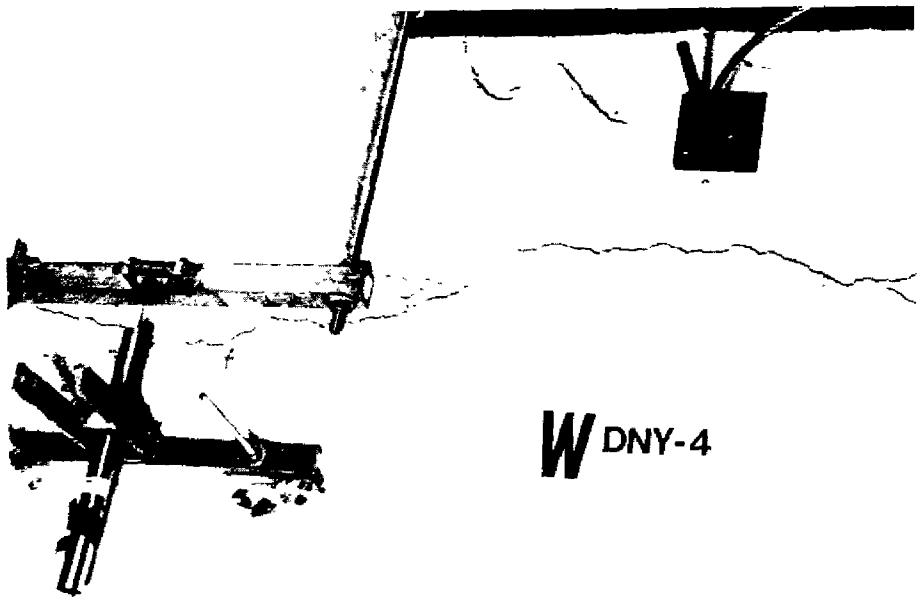

FIGURE 5-2 Flexural Yield Line at the Face of Spandrel Beam

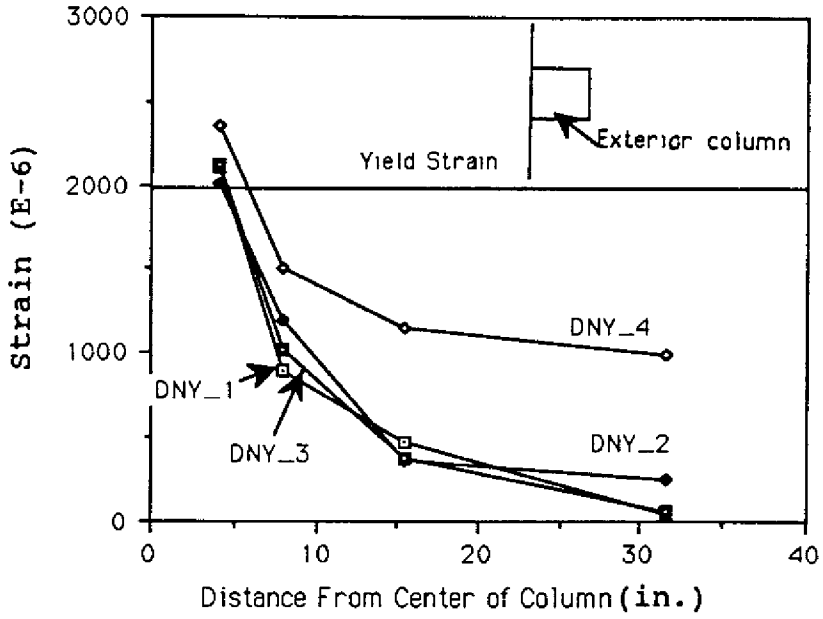

FIGURE 5-3 Strain Distribution at Yield of Exterior Connections

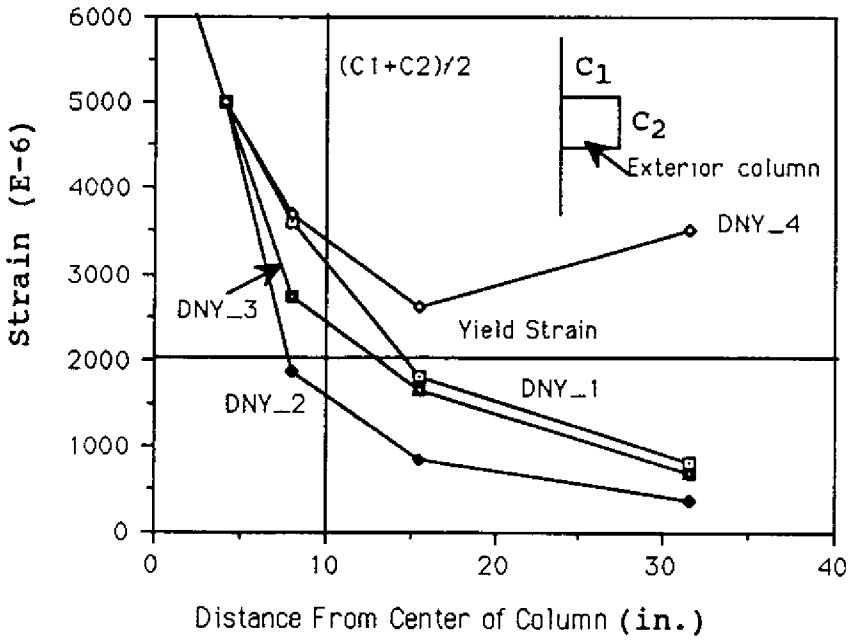

FIGURE 5-4 Strain Distribution at Peak Load of Exterior Connections

uniform distribution of strain in the slab and resulted in yielding of reinforcement in the entire slab width. In specimens without an edge beam, only the rebars within a certain distance centered on the column line yielded. Based on the configuration of the cracking pattern at the exterior connection and the variation of the observed strain, the reinforcement within a distance approximately equal to c_1+c_2, as indicated in figure 5-4, appears to participate fully in resisting the bending moment in specimens without a spandrel beam.The strain in reinforcement outside this region were below yield level and varied with each specimen. The specimen DNY_2 had the lowest strain level because of an early punching failure before the slab could develop its full strength.

5.3 Failure Mode

None of the exterior connections failed in punching shear. Low flexural and torsional stiffness of the slab at the exterior connection redistributed the load to the interior connection and thus protected the exterior connections from high shear stresses. The failure mode of exterior connections can be described only if a certain minimum performance criterion is specified. One may, however, look at the distinct yield mechanisms observed during the tests. Flexural mechanism controlled the response of the exterior connection in DNY_4 which had a spandrel beam. Flexural-torsional mechanism of the slab edge dominated the lateral load response of the connections without a spandrel beam. The anchorage failure of the slab bottom reinforcement was observed in all specimens. The exterior connection in DNY_2 did not reach the ultimate yielding mechanism because of the punching failure at the interior connection at 2% drift at which time the test was terminated.

5.4 Moment-Rotation Response

The anchorage of slab bottom reinforcement played a key role in the moment-rotation response of the exterior connections. The small amount of slab bottom reinforcement continuing into the connection region resulted in unsymmetrical hysteresis loops, and the anchorage failure caused excessive rotation of the slab under positive bending.

Typical moment-rotation loops of exterior connections are shown in figures 5-5 and 5-6. The moment-rotation response for exterior connections was affected both by the intensity of the gravity load and the presence of spandrel beams. Rotation of the slab in the connection region depended on the location of the flexural crack due relative to the column face under positive bending. The flexural crack on the bottom of the slab occurred adjacent to the column when slab bottom reinforcement yielded and lost its anchorage. When heavier gravity load created high negative moment in the connection region, flexural cracking under positive moment occurred a certain distance away from the column face. In the latter case, the slab bottom reinforcement may not lose its anchorage. This behavior can be noticed in the moment-rotation loops of DNY_1 and DNY_2 shown in figures 5-5 and 5-6. In DNY_1, the flexural crack in the slab under positive bending occurred very

near the column face and the slab reinforcement yielded and lost its anchorage rapidly as can be seen from the three distinct regions of stiffness change in figure 5-5. The first peak corresponds to cracking of the slab with second peak representing yielding of the reinforcement and beginning of the anchorage loss. This is followed by the third region which corresponds to total loss of anchorage resulting in large rotation of the slab. Flexural cracking at the bottom of the slab in DNY_2 occurred a certain distance away from the exterior column face and thus the slab bottom reinforcement was not as severely stressed as in DNY_1. The moment-rotation response under negative bending, which caused tension in the slab top reinforcement, was approximately bilinear in both cases. The yield point was relatively well defined as in under reinforced members. The slope of the second branch of the envelop, however, was distinctly different in the two cases. When the total loss of anchorage occurred, as in DNY_1, the slope is negative showing strength degradation. The anchorage in DNY_2 was not quite as severely affected as explained previously. The connection was able to retain its strength as indicated by positive slope of the second branch of the envelope in figure 5-6.

The moment-rotation response in the positive moment direction under dominant lateral load condition is of particular interest. Specimens DNY_1, DNY_3, and DNY_4 fall in this category. The hysteresis loops are highly unsymmetrical and very much dependant upon the behavior of connection under reversed bending.

5.5 Stiffness

The variation of stiffness of the four exterior connections during lateral loading is shown in figure 5-7. These plots show the secant stiffness based on the rotation of the slab over a distance of 6 inches from the column face. Due to significantly different reinforcement amounts and their anchorage detail in the top and bottom of the slab, the degradation of stiffness in the two directions differed considerably.

The specimen DNY_2, which carried the full dead and live load, had the highest initial stiffness in the loading direction that caused tension in the slab top reinforcement. This was followed by specimen DNY_4 with a spandrel beam and DNY_1 with bent-up slab reinforcement. The specimen DNY_3 with straight rebars in the slab had the least initial stiffness of all specimens. Approximately 70 to 75% of the initial stiffness was lost by 1% drift in all specimens. The rate of loss of stiffness decreased beyond 1% drift, with less than 10% of the initial stiffness remaining by the end of the test. The loss of stiffness in the negative bending direction resulted mostly from early yielding of the slab reinforcement.

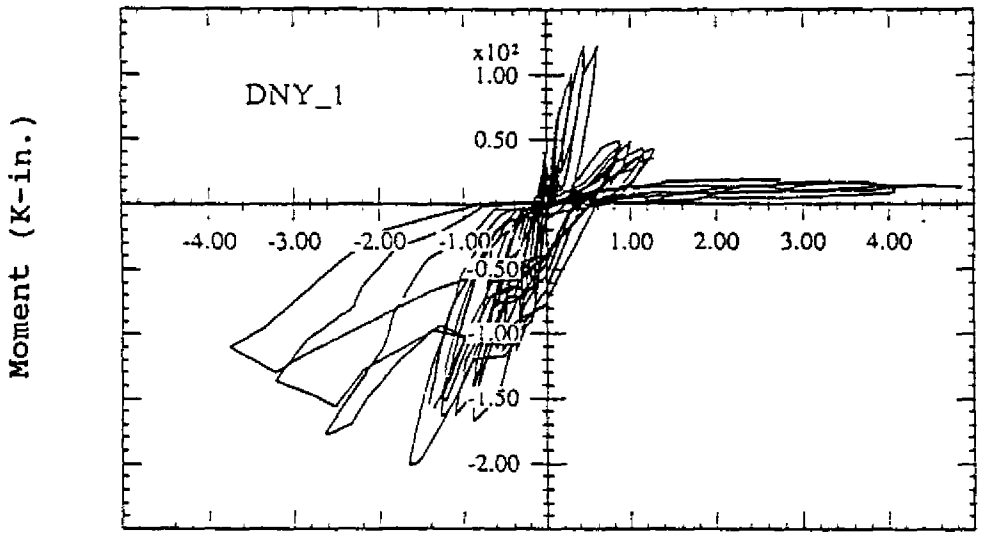

FIGURE 5-5 Moment-Rotation Response of Exterior Connection of DNY_1

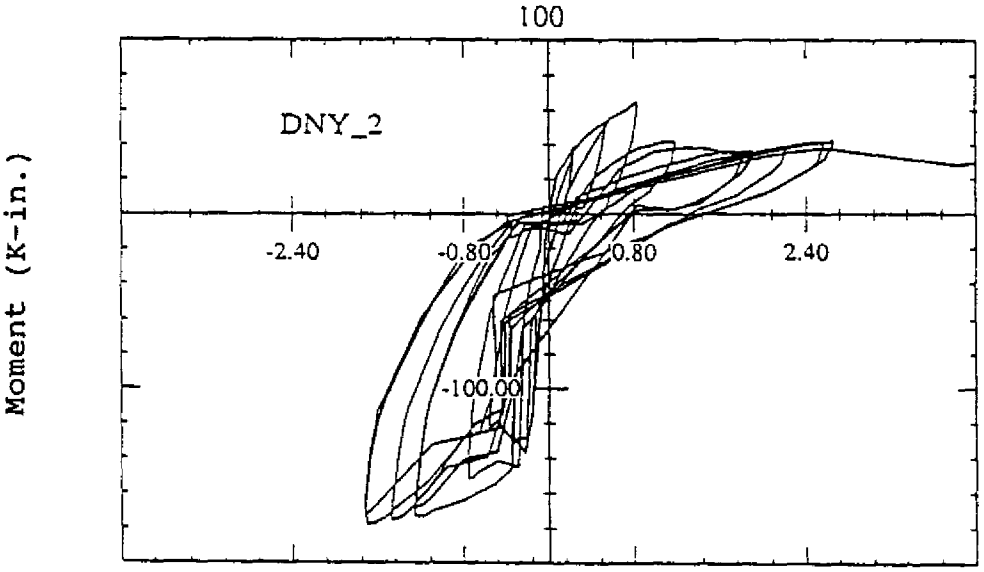

FIGURE 5-6 Moment-Rotation Response of Exterior Connection of DNY_2

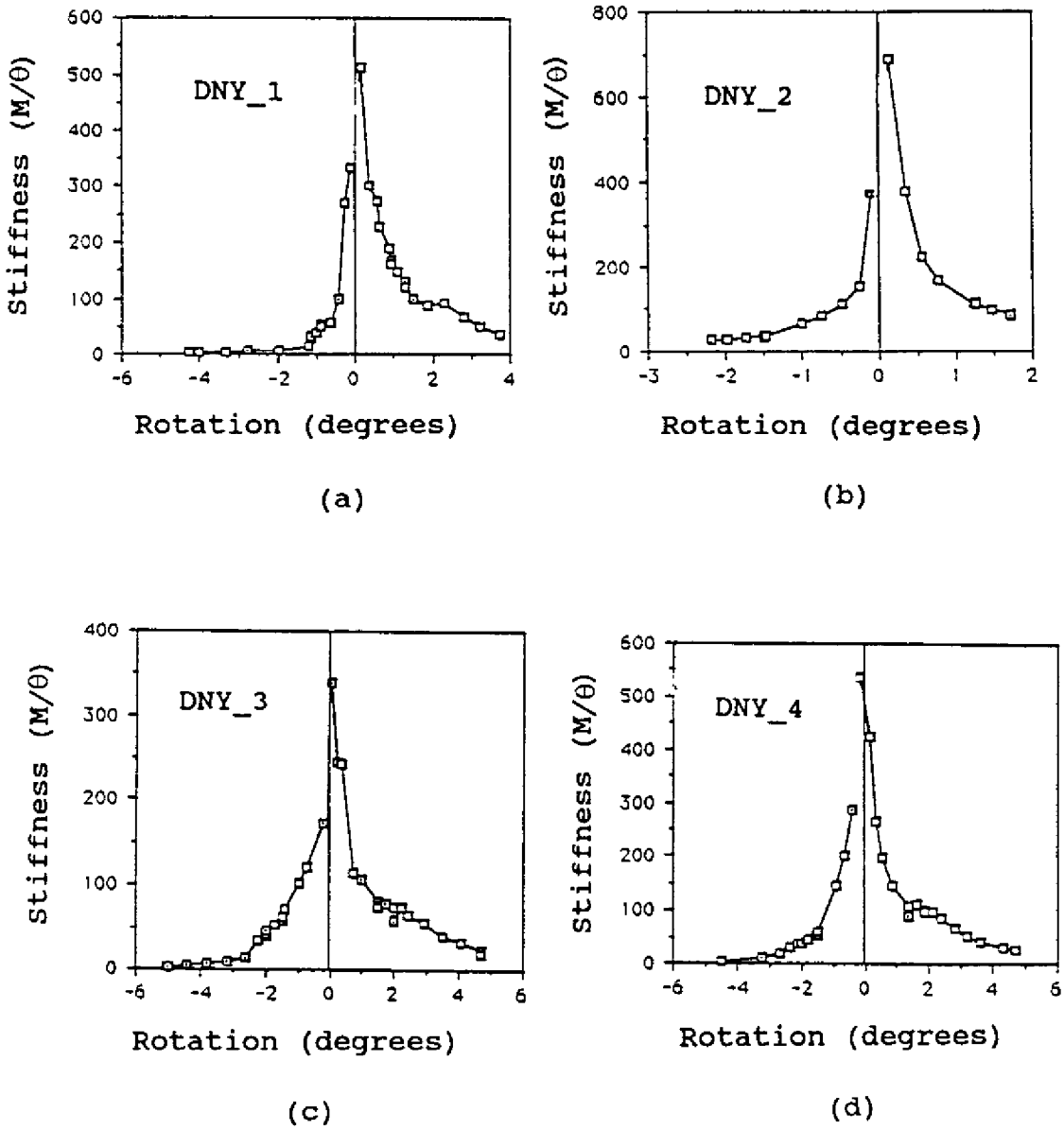

FIGURE 5-7 Stiffness Degradation of Exterior Connections

Rapid degradation of stiffness in the positive moment direction is attributed to anchorage failure of the slab bottom reinforcement. As soon as the slab reached its cracking strength, the slab bottom reinforcement yielded and stiffness dropped to less than 10% of the initial stiffness. With few additional reversals, anchorage of the slab bottom reinforcement was completely lost and the stiffness of exterior connections in the positive moment direction degraded to zero for all practical purposes. Specimen DNY_2, which supported the heavier gravity load, was an exception. The cracking moment in the slab occurred some distance away from the column face with less demand on anchorage and hence the loss of stiffness was more gradual.

5.6 Moment-Transfer Capacity

SLAB TOP IN TENSION

Two different moment-transfer mechanisms were observed at exterior connections. When a spandrel beam was present, flexural yield line developed across the full width of the slab and hence most of the slab participated in the transfer of moment between the column and the slab. At connections without an edge beam, the moment-transfer occurred through a flexural-torsional mechanism with very little or no effect of the reinforcing configuration of the slab. The relative strength of the slab edge in torsion and the flexural strength of the slab appear to control the mode of moment-transfer between the slab and the column. Figure 5-8 illustrates the two mechanisms observed during the tests. The first case, shown in figure 5-8(a), represents the spandrel beam case (DNY_4) where the cracking torsional capacity of the spandrel beam T_c was greater than the net slab flexural capacity $(M_s - M_{c1+c2})/2$ where M_s is the flexural capacity of the entire slab width and M_{c1+c2} is the flexural capacity of the slab over a width of $c1 + c2$ centered on the column line as indicated in figure 5-9. The moment in this case is transferred over the full slab width. With a strong spandrel beam, as in specimen DNY_4, the full width of the slab was effective as indicated by the distribution of strain in the slab reinforcement. The measured values of the moment transferred at the connection and the theoretical flexural capacity of the entire slab width are given in table 5-I. The ratio between the measured and the calculated moment capacities is 1.06 which strongly suggests full participation of the slab at exterior connections having a strong spandrel beam.

The second type of mechanism develops with a weak spandrel beam or no spandrel beam as in specimens DNY_1, DNY_2, and DNY_3. The torsional cracking strength of the slab edge is smaller than the flexural capacity of the slab and the slab edge reaches its torsional capacity before the slab is able to develop its full strength. The moment transfer, therefore, occurs through a combination of flexural-torsional mechanism as shown in figure 5-8(b). The crack pattern, failure mechanism, and strain distribution in the slab (figure 5-4) of specimens DNY_1, DNY_2 and DNY_3 suggest moment transfer to occur mostly over a slab width of c_1+c_2, where c_1 and c_2 are the column

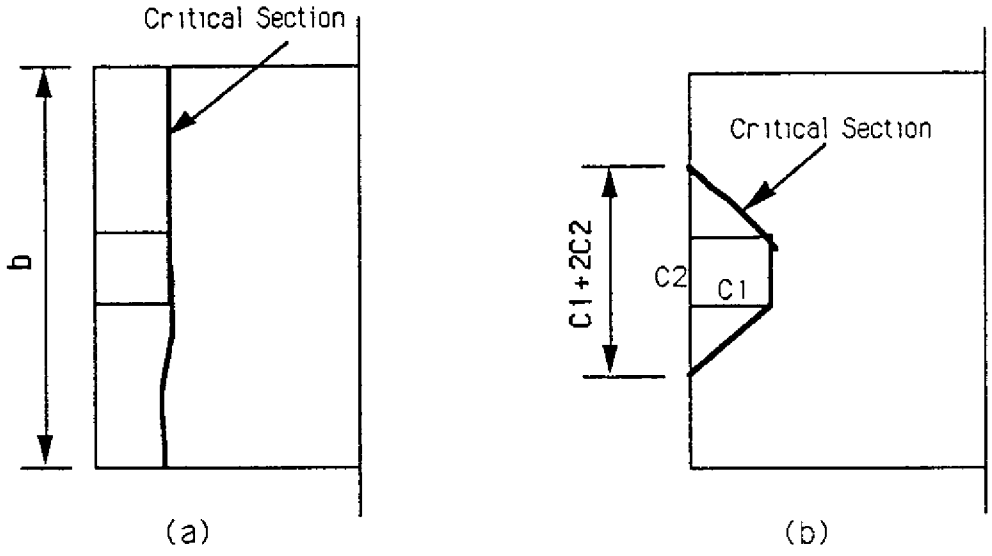

FIGURE 5-8 Critical Section at Exterior Connections

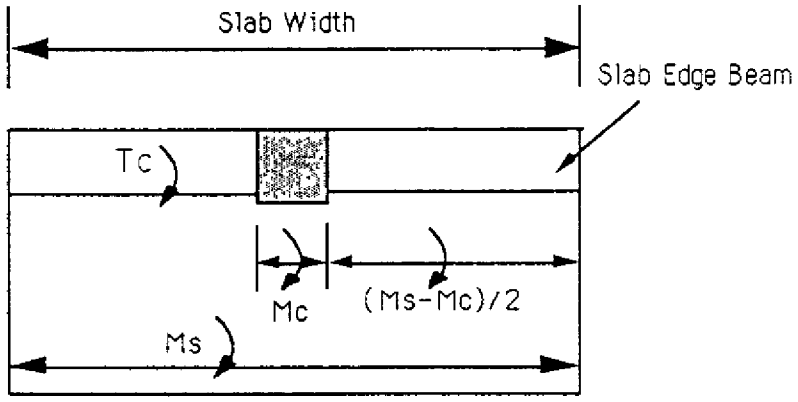

FIGURE 5-9 Moment-Transfer at Exterior Connections

dimensions perpendicular and parallel to the loading direction, respectively. The total moment transfer capacity, therefore, consists of two components: (a) the flexural capacity of the slab width equal to c_1+c_2, (b) the torsional capacity of the slab edge on both sides of the column i.e.

$$M_{total} = M_{c1+c2} + 2T_c$$

where M_{c1+c2} is the slab contribution and T_c is the torsional cracking strength of the slab edge as shown in figure 5-8.

TABLE 5-I Negative Moment-Transfer Capacity of Exterior Connections

Connection	Measured		Calculated		Measured/ Calculated
	M_{mf}*	Effective Slab Width	M_n†	$2T_c+M_{c1+c2}$ ‡	
DNY_1W	158	c_1+c_2	249	130	1.22
DNY_1E	177	c1+c2	249	130	1.36
DNY_2W	119	c1+c2	243	123	0.97
DNY_2E	106	c1+c2	243	123	0.86
DNY_3W	158	c1+c2	242	122	1.29
DNY_3E	160	c1+c2	242	122	1.31
DNY_4W	255	full width	240	265	1.06
DNY_4E	258	full width	240	265	1.08

*. measured maximum moment at column face, k-in.
†. nominal negative flexural capacity of full slab width, k-in.
‡. torsional strength of edge beam plus flexural strength of c_1+c_2 width of slab

Since the slab edge is not reinforced with closed stirrups for the steel to be effective in resisting torsion, the torsional capacity of the slab edge is limited to its cracking torsional strength T_c, which may be calculated by

$$T_c = \alpha\sqrt{f_c'}\frac{\Sigma x^2 y}{3}$$

where α factor has a value between 4.0 and 7.0. ACI Building Code (11) conservatively uses a factor of 2.4 which corresponds to a torque equal to about 40% of the cracking torque of a beam without web reinforcement with implied α factor of 6.0. To calculate the theoretical capacity of

the slab edge, α is assumed as 5.0 (ref. 14-18). A comparison of the total calculated moment-transfer capacity and the moment-transfer observed at the edge connections is shown in table 5-I. This approach results in theoretical capacity to be approximately 90% of the measured moment-transfer capacity

SLAB BOTTOM IN TENSION

The amount and anchorage of slab positive reinforcement at the exterior connections affected both the failure mechanism and the moment-transfer capacity under positive bending. In specimens DNY_1, DNY_2 and DNY_3, which had bent-up bar configuration in the slab, one third of the slab bottom reinforcement (ρ_{bottom} = 0.11%) at mid-span extended into edge connections (4). This amount of reinforcement is less than the minimum reinforcement necessary for the flexural capacity to be higher than the cracking moment capacity of the slab at column face. The moment transfer under positive bending is, therefore, limited to the cracking strength of the entire slab width.

In straight bar configuration in the slab, as in DNY_3, all of the slab bottom reinforcement extended into the slab edge. Thus, the cracking pattern and the mechanism of moment- transfer under positive bending was very similar to that observed under negative bending i.e. a flexural-torsional mechanism of moment-transfer. The maximum effective width of the slab was limited to $c1 + c2$ as for the case with slab top reinforcement in tension. The procedure described previously for moment-transfer under negative bending could also be used in this case. The total moment-transfer capacity under positive bending for the straight bar configuration in the slab may be taken as the flexural strength of the slab width equal to $c1 + c2$ plus the torsional strength of the slab edge.

Depending upon the magnitude of the gravity load, the cracking of the slab under positive bending may occur a certain distance away from the column face. Under full dead and live load, as in specimen DNY_2, the net positive moment at the face of the column was less than the cracking moment. The moment in the slab reached the cracking capacity approximately 20 inches from the column face, hence the measured moment was approximately one-half the cracking capacity as shown in table 5-II. With bent-up reinforcing detail, the moment-transfer capacity under positive bending is limited to cracking strength of the slab. Furthermore, once the slab reaches its cracking strength, the positive moment-transfer capacity of the connection degrades rapidly. When a stiff edge beam is present, M_{cr} underestimated the moment-transfer by approximately 25% and it over estimated the observed capacity by 13% when slab is without an edge beam.

TABLE 5-II Positive Moment-Transfer Capacity of Exterior Connections

Connection	Measured		Calculated		Measured/ Calculated
	M_{mf}*	Effective Width	M_{cr}†	$2T_c+M_{c1+c2}$	
DNY_1W	125	full width	147	n/a	0.85
DNY_1E	132	full width	147	n/a	0.90
DNY_2W	67	‡	137	n/a	0.49
DNY_2E	70	**	137	n/a	0.51
DNY_3W	103	c_1+c_2	n/a	97	1.06
DNY_3E	108	$c1+c_2$	n/a	97	1.11
DNY_4W	138	full width	112	n/a	1.23††
DNY_4E	146	full width	112	n/a	1.30

*. measured maximum moment at column face, k-in.
†. slab cracking moment, k-in.
‡. connection did not reach its full moment-transfer capacity because of punching at interior connection
**. same as above
††. higher measured capacity due to strain hardening effect from stiff edge beam

5.7 Anchorage Performance

Approximately one-third to one-half of the slab bottom reinforcement at midspan was extended into exterior connections in specimen DNY_1, DNY_2 and DNY_4. The embedment length of these rebars into the column was six inches. To evaluate the anchorage performance, two strain gages were attached to the bar, one at the column face (point 1) and the other at 1.5 inches (point 2) from the end of the rebar. The observed variation of strain at these two locations for specimen DNY_1 is shown in figure 5-10. Before the slab reached its cracking strength at the column face, the strain at point 2 was nearly zero. When the slab developed a main flexural crack at about 1.5% drift, the point 1 reached the yield strain and the strain increased rapidly. At about 2.25%, the rebar lost its anchorage as indicated by the sudden drop in strain at point 1 and a small increase in strain at point 2. At this stage, the bar began to slip and it could resist only a small force due to friction between the steel and concrete. The slippage of the bar resulted in a significant increase in the rotation of the slab relative to the column face and the connection lost its stiffness in positive bending. The rotation of the slab at 2.25% drift was approximately 2.5 times the rotation at first yield.

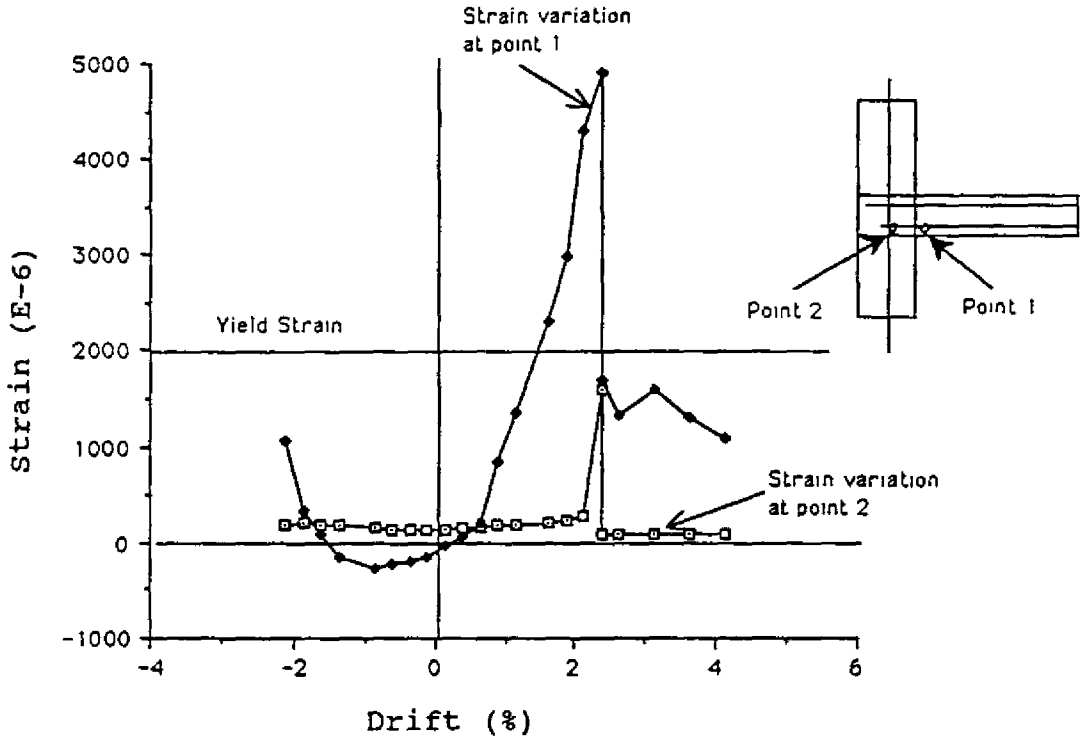

FIGURE 5-10 Variation of Anchorage Strain With Drift

Comparing EPF to prototype frequency, the accuracy of the scaled down model was determined. Examining Table 5-II, it can be seen that most of the EPF's are higher than the prototype frequency. This was expected by the authors since the prototype was built in the field, thus the assumption of fixed end column is not as rigidly defined as in the model. Also, soil-structure interaction was another factor contributing to the lower natural frequency of the prototype. Therefore, the result obtained is quite satisfactory except for the "F" frame in Y-Y direction.

The fundamental frequency change due to the inclusion of different bracing systems is obvious. The stiffness increase can be expressed in relation to the change of fundamental natural frequency if the structure is idealized as a one DOF structure system. The stiffness change from "F" to "E" can be calculated in the following form:

$$\frac{K_F}{K_E}=\left(\frac{f_E}{f_F}\right)^2=4.92 \tag{5.2}$$

The increase of stiffness is apparent by adding different bracing. The change of stiffness is 4.92 for E bracing, 7.19 for V bracing, and 8.19 for X bracing.

Note that in the "F" case, the prototype has a natural frequency higher than the EPF. This is contrary to what is described above. Explanation of this phenomenon was sought and it was found that model construction was the cause of this discrepancy. It was described in Section 3.4, referring to Figure 3-8, that discrepancy between model and prototype does exist. The missing stiffener on the column would have contributed some extra stiffness to the structure. Had this stiffener been included in the model, the natural frequency of the model would be increased, since the column rigid zone in the model is lengthened by the combined action of the gusset plate and stiffener. This missing stiffener apparently is not as important in the braced structures, since bracing itself provides most of the stiffness to the structure. However, the bare frame structure relies entirely on the rigidity of its beams and column for stiffness.